

Research Article

The dusty aftermath of a rapid nova: V5579 Sgr

Ashish Raj¹, Mohit Singh Bisht¹, F.M. Walter², R. Pandey³, C.E. Woodward⁴, D.E. Harker⁵, Devendra Bisht¹, H.P. Singh⁶, A. Agarwal⁷, Jeewan Pandey⁸, Arti Joshi⁹, K. Belwal¹ and Christian Buil¹⁰

¹Indian Centre for Space Physics, Kolkata, West Bengal, India, ²Department of Physics and Astronomy, Stony Brook University, Stony Brook, NY, USA, ³Physical Research Laboratory, Navrangpura, Ahmedabad, Gujarat, India, ⁴Minnesota Institute for Astrophysics, University of Minnesota, Minneapolis, MN, USA, ⁵Department of Astronomy and Astrophysics, University of California, San Diego, La Jolla, CA, USA, ⁶Department of Physics and Astrophysics, University of Delhi, Delhi, India, ⁷Center for Cosmology and Science Popularization(CCSP), SGT University, Budhera, Delhi, NCR, India, ⁸Aryabhata Research Institute of Observational Sciences (ARIES), Manora Peak, Nainital, India, ⁹Institute of Astrophysics, Pontificia Universidad Católica de Chile, Santiago, Chile and ¹⁰Castanet Tolosan Observatory, Castanet Tolosan, France

Abstract

V5579 Sgr was a fast nova discovered in 2008 April 18.784 UT. We present the optical spectroscopic observations of the nova observed from the Castanet Tolosan, SMARTS, and CTIO observatories spanning over 2008 April 23 to 2015 May 11. The spectra are dominated by hydrogen Balmer, Fe II, and O I lines with P-Cygni profiles in the early phase, typical of an Fe II class nova. The spectra show He I and He II lines along with forbidden lines from N, Ar, S, and O in the nebular phase. The nova showed a pronounced dust formation episode that began about 20 days after the outburst. The dust temperature and mass were estimated using the WISE data from spectral energy distribution (SED) fits. The PAH-like features are also seen in the nova ejecta in the mid-infrared Gemini spectra taken 522 d after the discovery. Analysis of the light curve indicates values of t_2 and t_3 about 9 and 13 days, respectively, placing the nova in the category of fast nova. The best-fit CLOUDY model of the early decline phase JHK spectra obtained on 2008 May 3 and the nebular optical spectrum obtained on 2011 June 2 shows a hot white dwarf source with $T_{BB} \sim 2.6 \times 10^5$ K having a luminosity of 9.8×10^{36} ergs s^{-1} . Our abundance analysis shows that the ejecta is significantly enhanced relative to solar, O/H = 32.2, C/H = 15.5, and N/H = 40.0 in the early decline phase and O/H = 5.8, He/H = 1.5, and N/H = 22.0 in the nebular phase.

Keywords: Stars: novae; cataclysmic variables; stars: individual (V5579 Sgr); techniques: spectroscopic; line: identification

(Received 28 May 2024; revised 17 July 2024; accepted 1 August 2024)

1. Introduction

Classical novae (CNe) are explosive events characterised by a sudden and substantial increase in brightness of a primary white dwarf (WD) star in a semi-detached binary star system. The WD accretes hydrogen-rich matter from its companion via an accretion disc. This mass transfer is made through an inner Lagrange point (L_1). The material accumulates on the surface of the WD, until eventually the matter at the base of the accreted envelope undergoes runaway nuclear fusion reactions, releasing an immense amount of energy and causing the luminosity of the underlying binary system to increase upto 10^4 – 10^5 L_\odot . The luminosity of the quiescence stage generally ranges from a few times to several hundreds times L_\odot (Bode & Evans 2008). Approximately 10^{-4} – 10^{-5} M_\odot of nuclear-processed material is ejected into the interstellar medium (ISM), typically at velocities ranging from a few hundred to several thousand kilometres per second (Bode & Evans 2008; José, Shore, & Casanova 2020; Starrfield et al. 2020, and references therein). CNe also serves as the main contributor

of ^{13}C , ^{15}N , and ^{17}O within the Galaxy, potentially influencing the abundance of other isotopes in the intermediate mass range, such as ^7Li and ^{26}Al (Starrfield et al. 2020).

Nova V5579 Sgr was discovered during eruption in 2008 April 18.784 UT by Nishiyama and Kabashima (Nakano et al. 2008) at $V = 8.4$. Munari et al. (2008) reported a rapid and steady brightening of about 0.7 mag/d in the initial stages of V5579 Sgr. The nova reached its maximum brightness of $V_{\text{max}} = 6.61$ on 2008 April 23.394 UT approximately 4.6 days after discovery. A BVRCIc photometric sequence around V5579 Sgr was reported by Henden & Munari (2008). They found that the field is extremely crowded, with several very faint field stars lying within 4 arcsec of the nova position, and it was not listed in the United States Naval Observatory B1 (USNO B1) or Two Micron All Sky Survey (2MASS) catalogs. Astrometry was performed using subprogram Library (SLALIB) (Wallace 1994) linear plate transformation routines in conjunction with the Second U.S. Naval Observatory CCD Astrograph Catalog (UCAC2). The astrometric fit was less than 0.3 arcsec.

Archival photometry was performed by Jurdana-Sepic & Munari (2008) for the nova. The Asiago Schmidt plate archive was searched for V5579 Sgr and 106 plates were found that covered its position. After plate inspection, 58 good B and Ic band plates were finally retained. These 58 good plates covered the period 1961 June

Corresponding author: Ashish Raj; Email: ashishpink@gmail.com

Cite this article: Raj A, Bisht MS, Walter FM, Pandey R, Woodward CE, Harker DE, Bisht D, Singh HP, Agarwal A, Pandey J, Joshi A, Belwal K and Buil C. (2024) The dusty aftermath of a rapid nova: V5579 Sgr. *Publications of the Astronomical Society of Australia* 41, e051, 1–14. <https://doi.org/10.1017/pasa.2024.65>

16 to 1977 July 24, with an average limiting magnitude $B \sim 18$, $I_c \sim 15.5$. They found that the progenitor was below the limiting magnitude on all plates. A search of pre-eruption object in the Digitized Sky Survey (DSS) red image from 1991 and UK Schmidt red plate obtained on 1996 September 08 by Dvorak, Guido, & Sostero (2008) did not reveal any object at the position of V5579 Sgr. With the limiting magnitude of these surveys close to 20 mag, V5579 Sgr is one of the largest amplitude ($\Delta V = 13$ mag) observed novae in recent years.

The optical spectrum taken one day after the discovery by Yamaoka, Haseda, & Fujii (2008) showed hydrogen Balmer series absorption lines, with a prominent P-Cygni profile in the $H\alpha$ line in addition to several additional broad absorption lines. Infrared (IR) spectra reported by Raj, Ashok, & Banerjee (2011), Russell et al. (2008), and Rudy et al. (2008) showed lines of O I, N I, Ca II and strong lines of C I. The full width at half maximum (FWHM) of the lines was estimated as $1\,600\text{ km s}^{-1}$. The NIR spectrophotometric evolution of the nova from 5 days to 25 days after discovery was presented by Raj et al. (2011). The JHK band spectra taken around the maximum show prominent lines of hydrogen, neutral nitrogen, and carbon and show deep P-Cygni profiles. Dust formation was reported both by Rudy et al. (2008) and Raj et al. (2011), which is consistent with the presence of spectral lines of low-ionisation species such as Na I and Mg I in the early spectra, as they are believed to be indicators of low-temperature zones conducive to dust formation in the nova ejecta. Dust formation was also seen from the light curve as a sudden increase in the rate of decay in the V band brightness after about 20 days after the outburst. The *Neil Gehrels Swift Observatory* observed V5579 Sgr during six epochs from 2008 April 28 to 2009 July 31, with no X-ray detection (Schwarz et al. 2011).

The paper is organised as follows. Section 2 presents the details of the observations. Section 3 investigates the evolution of optical spectra from days 4 to 2 578 post-outburst. This section also includes a comprehensive analysis of the nova, estimation of crucial physical and chemical parameters using photoionisation modelling, along with a discussion on dust using archival low-resolution mid-IR Gemini spectra obtained 522 days post-outburst and WISE data. Finally, a comprehensive discussion in Section 4 and summary in Section 5 is provided.

2. Observations

Low-dispersion optical spectra were obtained using the Castanet Tolosan observatory in France and facilities of the Small and Moderate Aperture Research Telescope System (SMARTS) in Chile. The six low-dispersion spectra from the Castanet Tolosan observatory were obtained starting from near-peak brightness on 2008 April 23 through 2008 April 29. We obtained 15 spectra with the SMARTS R/C spectrograph on an irregular cadence from 2008 April 27 through 2011 July 28. The SMARTS R-C grating spectrograph, data reduction techniques, and observing modes are described by Walter et al. (2012). A final low-dispersion spectrum was obtained on 2015 May 11 using the COSMOS long slit spectrograph on the Cerro Tololo Inter-American Observatory (CTIO^a) Blanco 4m telescope. Data was reduced using standard IRAF procedures; spectra were extracted using software written in IDL. An

Table 1. Observational log for spectroscopic data obtained for V5579 Sgr.

| Date (UT) | Time since discovery (days) | Exposure time (s) | Wavelength range (Å) | Observatory |
|------------------|-----------------------------|-------------------|----------------------|-------------|
| 2008 April 23.08 | 4.31 | 240 | 4 293–6 856 | Tolosan |
| 2008 April 24.10 | 5.32 | 2 400 | 4 288–6 860 | Tolosan |
| 2008 April 25.09 | 6.31 | 1 500 | 4 290–6 857 | Tolosan |
| 2008 April 26.06 | 7.27 | 1 500 | 4 296–6 854 | Tolosan |
| 2008 April 27.09 | 8.13 | 2 400 | 4 722–6 865 | Tolosan |
| 2008 April 28.18 | 9.39 | 600 | 4 060–4 734 | SMARTS |
| 2008 April 28.38 | 9.59 | 900 | 3 869–4 543 | SMARTS |
| 2008 April 29.10 | 10.32 | 2 700 | 5 579–7 242 | Tolosan |
| 2008 April 29.34 | 10.55 | 1 200 | 3 870–4 544 | SMARTS |
| 2008 May 01.28 | 12.49 | 180 | 5 533–6 853 | SMARTS |
| 2008 May 03.35 | 14.57 | 1 200 | 3 871–4 545 | SMARTS |
| 2008 May 04.32 | 15.54 | 300 | 3 654–5 425 | SMARTS |
| 2008 May 10.14 | 21.36 | 1 200 | 4 061–4 735 | SMARTS |
| 2008 May 10.27 | 21.49 | 300 | 5 528–6 847 | SMARTS |
| 2008 May 11.25 | 22.47 | 300 | 3 655–5 426 | SMARTS |
| 2008 May 16.32 | 27.53 | 900 | 3 654–5 424 | SMARTS |
| 2009 Sept 23.04 | 522.26 | 642 | 77 000–140 000 | Gemini |
| 2011 May 17.37 | 1 123.58 | 2 700 | 5 631–6 950 | SMARTS |
| 2011 May 18.16 | 1 124.38 | 1 800 | 5 987–9 482 | SMARTS |
| 2011 June 02.17 | 1 139.39 | 2 700 | 2 760–9 600 | SMARTS |
| 2011 June 03.35 | 1 140.57 | 2 700 | 5 625–6 945 | SMARTS |
| 2011 July 28.22 | 1 195.43 | 3 000 | 5 996–9 490 | SMARTS |
| 2015 May 11.20 | 2 578.41 | 2 700 | 3 800–6 615 | CTIO |

observation of the spectrophotometric standard LTT 4364 was used to provide flux calibration.

2.1 Gemini South TReCs

Mid-IR $10\text{ }\mu\text{m}$ spectra of V5579 Sgr were obtained on September 23, 2009 00:58.33UT (Program GS-2009B-Q68) using the Thermal-Regions Camera Spectrograph (TReCS; De Buizer & Fisher 2005) imaging spectrograph on the 8 m Gemini South telescope on Cerro Pachon, Chile. Spectra were obtained with a $\simeq 0.65$ arcsec wide slit and the $10\text{ }\mu\text{m}$ Lo-Res grating, using standard IR chop-nodding observing techniques, under conditions of low relative humidity and measured seeing of $\simeq 0.32$ arcsec in the [N]-band (determined from the acquisition images). The V5579 Sgr spectra have a total exposure time of 642 s. The photometric standard was HD 151680. Raw data sets (two sets of spectra) were retrieved from the Gemini Observatory Science Archive Data^b for reduction following the methodology outlined in Harker et al. (2018). The spectra were flux calibrated using the average [N]-band flux value of 1.77 Jy calculated from acquisition image photometry. The spectra were integrated over the width of the [N]-band filter and ratioed to the calculated flux value.

The log of spectroscopic observations is given in Table 1.

^a<https://noirlab.edu/science/>.

^b<https://archive.gemini.edu/searchform>.

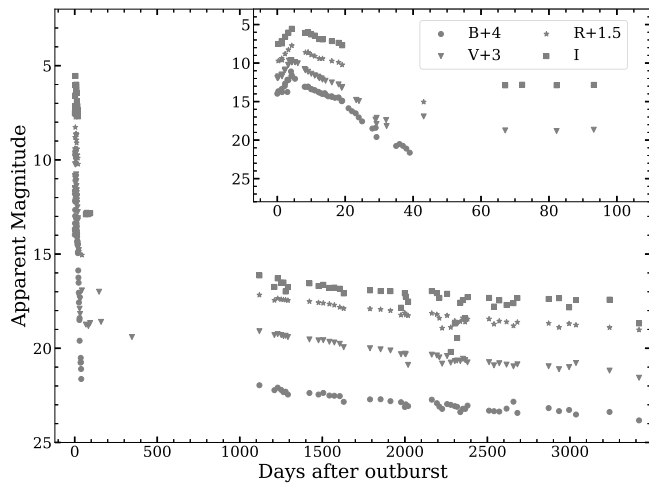


Figure 1. Optical light curves of V5579 Sgr generated using optical data from AAVSO and SMARTS. Offsets have been applied for all the magnitudes except *I* for clarity.

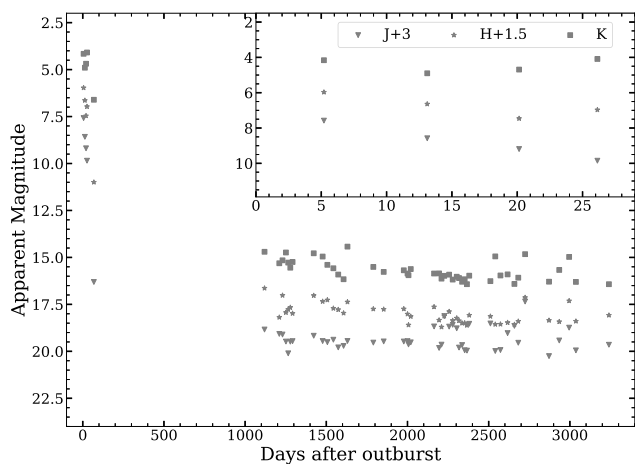


Figure 2. NIR light curves of V5579 Sgr generated using NIR data from Raj et al. (2011) and SMARTS. Offset have been applied for all the magnitudes except *K* for clarity.

3. Analysis

3.1 The pre-maximum rise, outburst luminosity, reddening, and distance

The optical and near-IR (NIR) light curves based on the American Association of Variable Star Observers (AAVSO^c) database (Kafka 2021), Raj et al. (2011) and the SMARTS Nova Atlas^d (Walter et al. 2012) database are presented in Figs. 1 and 2. Nova V5579 Sgr was first discovered on 2008 April 18.784 UT; in this paper, we considered this date as the day of the outburst (day 0). The BVRI band light curve begins within a day after discovery. The brightness increased at a fast rate for all bands and reached the peak magnitude $V_{\max} = 6.61 \pm 0.01$ after 4.6 days of the discovery. The brightness in the BVRI bands shows a moderate decline after the peak until day 18. A sudden increase in the decay rate was observed in the *B* and *V* bands after 19.6 days. The decay rate

was about 0.22 ± 0.03 mag/day, until 19.6 days, and changed to 0.39 ± 0.04 mag/day after 20 days. This clearly indicates dust formation in the nova ejecta (see Fig. 1). This is further supported by Fig. 2, which shows an increase in the brightness of the NIR *H* and *K* bands. The nova faded to >15 mag in *V* between 32 and 67 days from the outburst, suggesting that a large amount of dust was formed in the nova ejecta. We do not have any data between 350–1125 days, so we are not able to comment on recovery in the BVRI and JHK bands. Since day 1125 it has faded slowly, in optical and NIR which continued until our last observation at day 3419. The nova was at 19.8 ± 0.002 , 18.6 ± 0.001 , 17.5 ± 0.001 , 18.7 ± 0.001 , and 15.1 ± 0.01 , 17.1 ± 0.001 , 16.2 ± 0.001 mag in BVRI bands and JHK bands, respectively, on day 3419.

We derive the reddening to be $E(B - V) = 0.7 \pm 0.14$ from the mean value of all reported values (0.72, 0.82, and 0.56; Raj et al. 2011; Hachisu & Kato 2019; Hachisu & Kato 2021, respectively) towards the direction of the nova. We adopt $A_V = 2.2$ mag for extinction, assuming $R = 3.1$.

From the least-squares regression fit to the post-maximum *V* band light curve, we estimated t_2 to be 9 ± 0.2 days. Using the maximum magnitude versus rate of decline (MMRD) relation of Downes & Duerbeck (2000), we would expect that the absolute magnitude of the nova is $M_V = -9.3 \pm 0.1$ giving a distance modulus of $V_{\max} - M_V = 15.9$ mag. Using the distance modulus relation, we obtain a value of the distance $d = 5.6 \pm 0.2$ kpc to the nova. These estimated values of M_V and the distance are different from the estimates of Raj et al. (2011) mainly due to the different MMRD relation they used and the slight variation in the estimated value of t_2 .

These observed values of the amplitude $\Delta V = 13$ and $t_2 \sim 9$ days for V5579 Sgr are consistent with its location in the amplitude versus decline rate plot for CNe presented by Warner (2008), which shows $\Delta V = 12 - 15$ for $t_2 = 9$ days.

We have estimated the mass of the white dwarf (M_{WD}) using the derived value of the absolute magnitude M_V , t_3 from the relations given by Livio (1992). The mass of the underlying WD in V5579 Sgr is estimated to be $1.16 M_{\odot}$. The outburst luminosity is estimated from $M_{bol} = 4.8 + 2.5 \log(L/L_{\odot})$, where the bolometric correction applied to M_V is assumed to lie between -0.4 and 0.00 corresponding from A to F spectral types, respectively (novae at maximum generally have a spectral type between A to F). Using $M_V = -9.3$, we calculate the luminosity of the outburst $(5.34 \pm 0.97) \times 10^5 L_{\odot}$. A classification system for the optical light curves for novae on the basis of the shape of the light curve and the time to decline by 3 mag (t_3) from V_{\max} has been presented by Strope, Schaefer, & Henden (2010). The shape of the optical light curve of V5579 Sgr presented in Fig. 1 has all the characteristics of the D class of nova, which shows a dust dip in the *V* band light curve after the optical maximum. The early decline of V5579 Sgr following the rise to the maximum is interrupted by fast decline around 15 days after optical maximum and continues further. Thus, the classification of the optical light curve for V5579 Sgr is D(13), since the estimated value of t_3 is ~ 13 days for V5579 Sgr. The value t_3 obtained using the AAVSO *V* band light curve is slightly lower than the value obtained by the relation $t_3 = 2.75 (t_2)^{0.88}$, which gives $t_3 = 18.8$ days (Warner 1995). The small observed value of t_2 makes V5579 Sgr as one of the fastest Fe II novae in recent years. Other fast novae of Fe II class in recent years include N Aql 1999 (V1494 Aql, $t_2 = 6.6$ d, Kiss & Thomson 2000), N Sgr 2004 (V5114 Sgr, $t_2 = 11$ d, Ederoclite et al. 2006), N Cyg 2005 (V2361 Cyg, $t_2 = 6$ d, Hachisu & Kato 2007), N Cyg 2006 (V2362 Cyg,

^c<https://www.aavso.org/>.

^d<http://www.astro.sunysb.edu/fwalter/SMARTS/NovaAtlas/>.

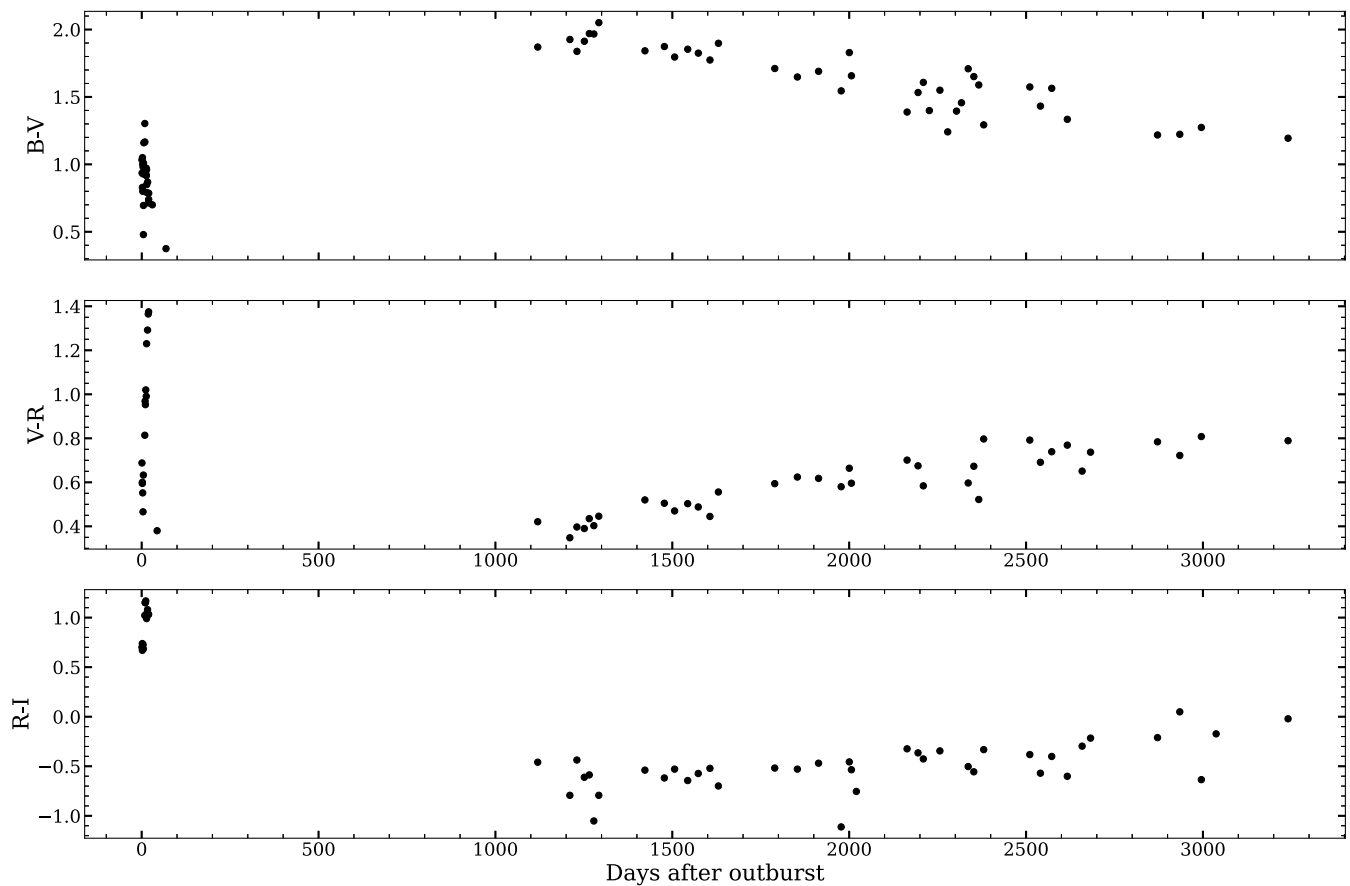


Figure 3. Evolution of Optical colour terms of nova V5579 Sgr from day 1 to day 3 240 since discovery.

$t_2 = 10.4$ d, Munari et al. 2008), N Oph 2006 (V2576 Oph, $t_2 = 8$ d, Schwarz et al. 2011), N Cyg 2007 (V2467 Cyg, $t_2 = 7$ d, Schwarz et al. 2011), and N Cyg 2008 (V2468 Cyg, $t_2 = 7.8$ d, Iijima & Naito 2011).

The NIR light curves are made using data from Raj et al. (2011) and the SMARTS/CTIO 1.3 m telescope facility (Walter et al. 2012). The NIR light curves are non-monotonic (Fig. 2). The *J* band light curves showed a steep, steady decline in the initial phase from the outburst, lagging the dust dip seen in the optical after day 20. But the *HK* band light curves showed an increase after 20 days from outburst, which is consistent with the dust formation as the dust mainly contributes at longer wavelengths (and the emission lines were not extremely strong Rudy et al. 2008). The *K* band light curve might have reached a peak value between 20 and 70 days after the outburst. After about day 20 the *K* band brightness increased by over 0.3 mag, accompanied by a smaller brightening in *H*, while *J* continued to fade. This can be taken as the start of dust formation. The *K* band magnitude brightened by 0.5 mag on day 26.

The *B-V*, *V-R*, and *R-I* colour evolution is shown in Fig. 3. The *B-V*, *V-R*, and *R-I* colours were approximately 1.03, 0.68, and 0.70, respectively, on day 1. By day 20, the *B-V* colour decreased to 0.74, while *V-R* and *R-I* increased to 1.36 and 1.03, respectively. Following this, *B-V* continued to decrease to 0.37 by day 68, and *V-R* decreased to 0.38 by day 43. There were no observations between days 68 and 1 119. On day 1 119, the *B-V*, *V-R*, and

R-I colours were approximately 1.87, 0.42, and -0.46 , respectively. From day 1 119 to day 3 240, *B-V* slowly decreased to 1.19, while *V-R* and *R-I* slowly increased to 0.79 and -0.02 mag, respectively. The *J-K* and *J-H* colour evolution is shown in Fig. 4. The *J-K* and *J-H* colours were about 0.4 and 0.1 at peak brightness, respectively. No colour excess was seen until 8 May 2008 (20.1 days since discovery), but a constant increase in the colours was clearly visible. The *J-K*, *J-H*, and *H-K* colours reach a maximum value of 6.7, 3.8, and 2.8, respectively, after 68 days from discovery which indicate that dust has been formed in the nova ejecta.

3.2 Line identification, general characteristics and evolution of the optical spectra

The optical spectra from SMARTS and the Castanet Tolosan Observatory, presented in Figs. 5 and 6, cover the early decline phase with 16 spectra and the nebular phase with five spectra. We presented 15 low-dispersion spectra using the SMARTS 1.5 m/RC spectrograph from 2008 April 28 (day 9) through 2011 July 27 (day 1 195), one low-dispersion spectrum obtained with the CTIO Blanco 4m COSMOS spectrograph on 2015 May 11 (day 2 578), and 6 low-dispersion spectra from Castanet Tolosan starting from peak brightness 2008 April 23 (day 4) to 2008 April 29 (day 10). The spectrum taken around peak brightness between 4–8 days shows deep P-Cygni profiles for the $H\alpha$ and $H\beta$ lines. The Na II doublets at 5 890 and 5 896 Å are also seen. The presence of large

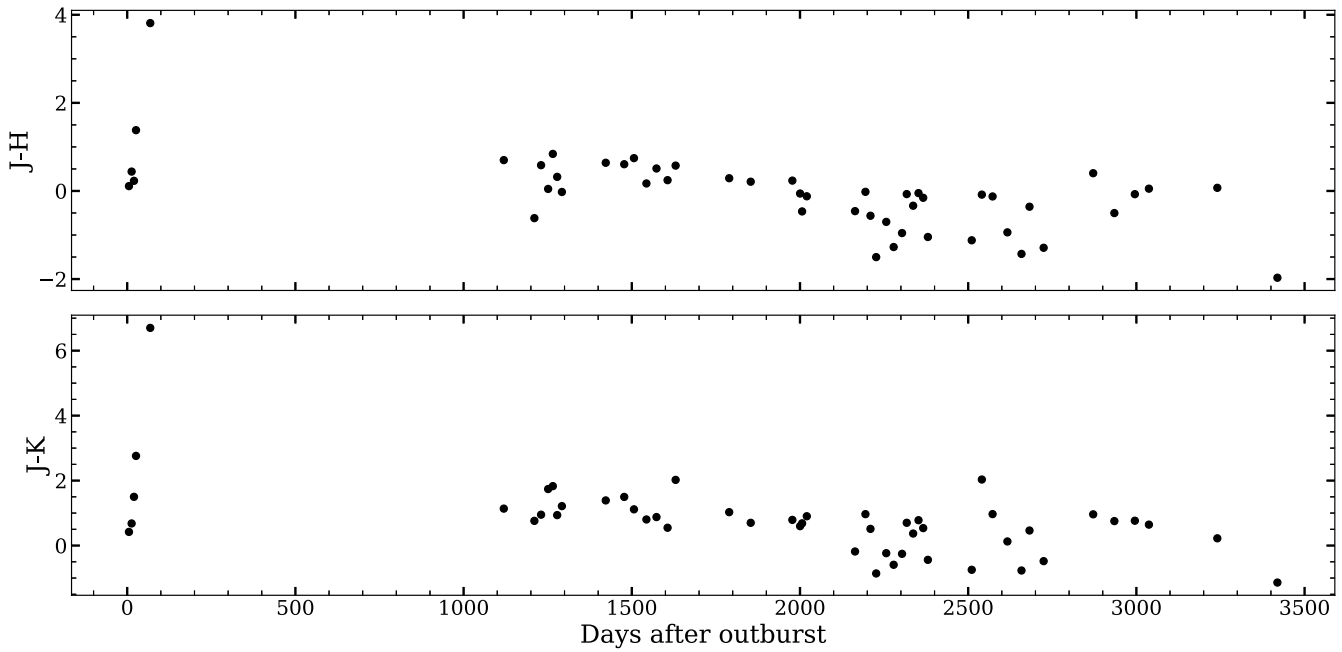


Figure 4. Evolution of NIR colour terms of nova V5579 Sgr from day 1 to day 3419 since discovery.

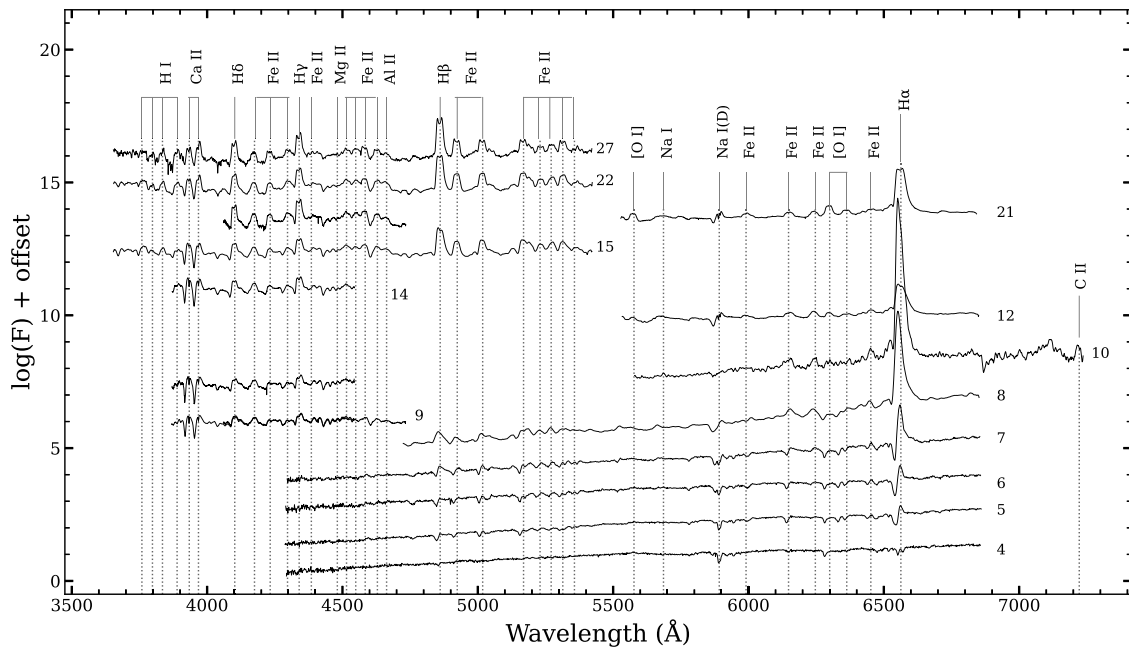


Figure 5. Low-resolution optical spectral evolution of V5579 Sgr obtained from day 4 (2008 Apr 23) to day 27 (2008 May 20). Spectra are dominated by Fe II multiplets and hydrogen Balmer lines. The lines identified are marked, and time since discovery (in days) is marked against each spectrum.

number of Fe II lines (5 018, 5 169, 5 235, 5 276, 6 148, 6 456 Å) in the initial phase indicates that the nova belongs to Fe II class. Most of the lines are seen in emission on day 9, for example, H I 4 102, 4 340 and Fe II 4 169, 4 233, 4 417, 4 458 Å. The spectra show the presence of hydrogen Balmer lines and Fe II multiplets along with Ca II (H and K) and He I at 5 876, [S II] at 6 716 Å. The ejecta velocity was estimated around 1 400–1 500 km s⁻¹ for hydrogen

lines. There was no significant change in the optical spectra until our last observations on day 27.

The emission lines grew progressively stronger and more complex with time. The Hydrogen Balmer and other metal lines were initially flat-topped, caused by the high line optical depth and later they developed ‘double-horn’ structure indicating that the total observed emission at a given wavelength arises from material

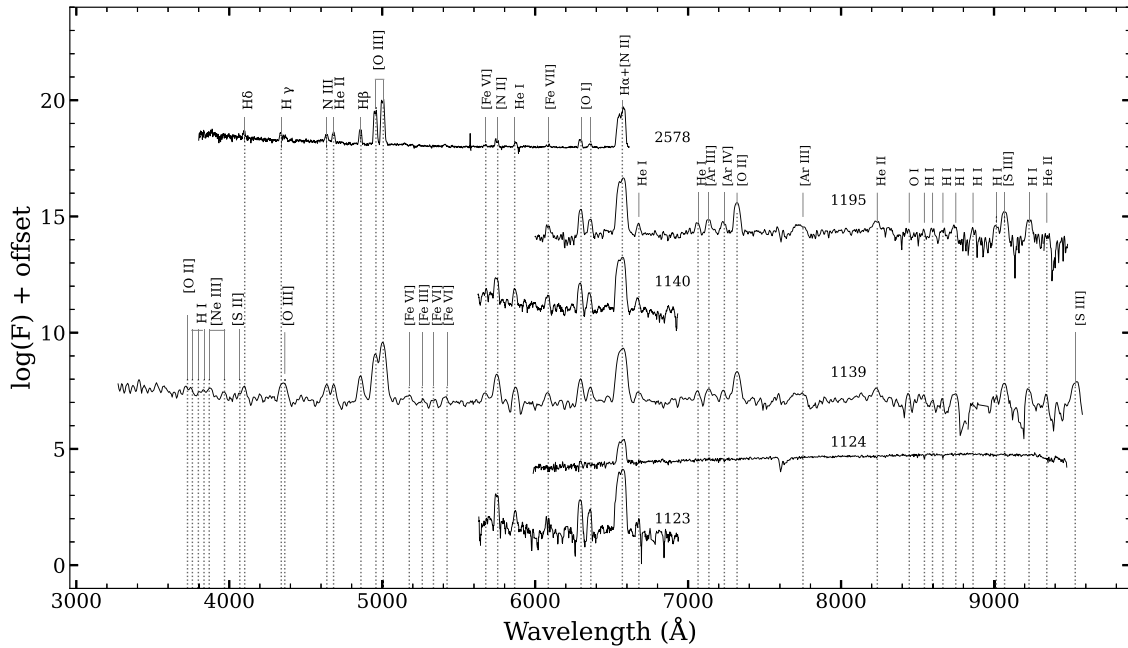


Figure 6. Low-resolution optical spectral evolution of V5579 Sgr obtained from day 1 123 (2011 May 17) to day 2 578 (2015 May 11). The [O I] lines at 6 300 and 6 363 Å are very prominent. Line identifications are marked, and time since discovery (in days) is marked against each spectrum.

receding from and approaching the observer (i.e. a ring or shell structure to the ejecta). The line profiles evolve from P-Cygni in the pre-maximum phase to a boxy and structured one in the decline phase. On day 27 for H α line the velocity peak of the blue-shifted material is of the order of $\sim -600 \pm 30 \text{ km s}^{-1}$, and the red-shifted material by $\sim 320 \pm 30 \text{ km s}^{-1}$. In the nebular phase (day 1 123) it changes to $\sim -560 \pm 20 \text{ km s}^{-1}$ for the blue-shifted and $\sim 670 \pm 20 \text{ km s}^{-1}$ for the red-shifted. In our last observations, the blue-shifted component decreased to $-470 \pm 30 \text{ km s}^{-1}$ the red-shifted to $590 \pm 30 \text{ km s}^{-1}$. Although we cannot ignore the contribution of the [N II] line at 6 584 Å.

The nebular phase spectra obtained after about 3 yr, on day 1 123, show higher excitation lines of [N II] 5 755, He I 5 876, [O I] 6 300, 6 363 and H α blended with [N II] 6 548 and [N II] 6 584 Å. The subsequent spectra taken on days 1 139 and 1 140 show emission lines of [O III] 4 363, 4 959, 5 007, [N II] 5 755, He II 4 686, [O I] 6 300, 6 363, He I 5 876, [O II] 7 320, and [S III] 9 069, 9 229 Å. In the final spectra the lines of [Ar III] 7 136, [Ar IV] 7 237, and He II 8 237 Å were present. The H α + [N II] lines are not clearly resolved, and [N II] 6 584 Å dominates the blend. The nova evolve in PFeAo sequence as per classification given by Williams et al. (1991). The only permitted lines are H β and H α and some He I and He II lines. Overall the spectrum resembles that of V2676 Oph some three years after its outburst (Raj, Das, & Walter 2017).

The day 2 578 spectrum is still nebular and is more excited. We see N III 4 640, He II 4 686 and 5 411, [Fe VII] 6 087, and a lot of other Nitrogen lines (5 460, 5 679 in addition to 5 755 and 6 548/6 584 Å).

The evolution of the H α velocity profile is as shown in Fig. 7. The P-Cygni profile was present until day 10. The P-Cygni profile of the H α line has a blue-shifted component at $\sim -500 \text{ km s}^{-1}$ on day 4, after which the bulk of the absorption shifted to $\sim -1 000 \text{ km s}^{-1}$.

3.3 Physical parameters

The physical parameters, for example, optical depth, electron temperature, density, and oxygen mass, can be estimated from the dereddened line fluxes of oxygen from the optical spectrum.

The optical depth of oxygen and the temperature of the electron are estimated using the formulas found in Williams (1994),

$$\frac{F_{\lambda 6 300}}{F_{\lambda 6 364}} = \frac{(1 - e^{-\tau})}{(1 - e^{-\tau/3})}. \quad (1)$$

Using the value of τ , the electron temperature (K) is given by

$$T_e = \frac{11 200}{\log \left[\frac{(43\tau)}{(1 - e^{-\tau})} \times \frac{F_{\lambda 6 300}}{F_{\lambda 5 577}} \right]} \quad (2)$$

where $F_{\lambda 5 577}$, $F_{\lambda 6 300}$, and $F_{\lambda 6 364}$ are the line intensities of [O I] 5 577, 6 300 and 6 364 Å lines. The optical depth τ of the ejecta for [O I] 6 300 Å is estimated to be about 0.23 on days 21 and 1 139. We do not see any change in the optical depth in three years of evolution. The electron temperature was estimated to be around 5 700 K for day 21 which is typically seen in novae (Ederoclite et al. 2006; Williams 1994). We have also estimated the electron density on day 1 139 (taking the typical value of $T_e \sim 10^4 \text{ K}$) using the [O III] 4 363, 4 959 and 5 007 Å lines in the following relation from Osterbrock & Ferland (2006)

$$\frac{j_{4 959} + j_{5 007}}{j_{4 363}} = 7.9 \frac{e^{3.29 \times 10^4 / T_e}}{1 + 4.5 \times 10^{-4} \frac{N_e}{T_e^{1/2}}} \quad (3)$$

In our low-resolution spectra [O III] 4 363 line was blended with H γ 4 340 Å, using the IRAF^c SPLIT deblending tool, the

^cNOIRLab IRAF is distributed by the Community Science and Data Center at NSF NOIRLab, which is managed by the Association of Universities for Research in Astronomy (AURA) under a cooperative agreement with the U.S. National Science Foundation.

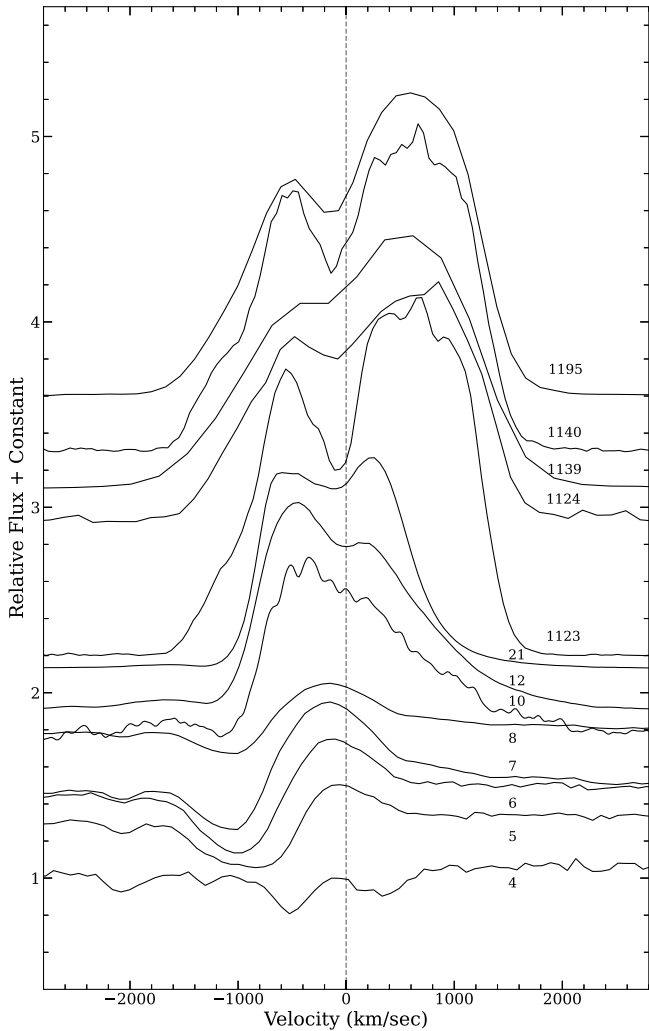


Figure 7. Evolution of H α velocity profile of V5579 Sgr from day 4 (2008 Apr 23) to 2 578 (2011 July 28) obtained using the low-resolution spectroscopic data. The line profiles evolve from P-Cygni in the pre-maximum phase to a boxy and structured one in the decline phase.

emission lines were deblended, and the flux for [O III] 4 363 Å was calculated. The electron density N_e was estimated as $5.42 \times 10^5 \text{ cm}^{-3}$. The oxygen mass can be estimated using the relation of Williams (1994),

$$\frac{m(O)}{M_\odot} = 152 d_{kpc}^2 \exp\left[\frac{22\,850}{T_e}\right] \times 10^{1.05E(B-V)} \frac{\tau}{1 - e^{-\tau}} F_{\lambda 6300} \quad (4)$$

The oxygen mass thus determined is found to be $3.8 \times 10^{-7} M_\odot$. Here we have used the distance estimated in Section 3.1.

3.4 Photoionisation modelling of optical and NIR spectra

We have used the photoionisation code CLOUDY, C23.01 (Chatzikos et al. 2023) to model the early phase NIR spectrum from Raj et al. (2011) and the nebular phase optical spectrum of V5579 Sgr taken on 2008 May 2 and 2011 June 2, 15 and 139 days, respectively, after the outburst. By choosing the ‘pre-dust’ (15 days) and ‘nebular phase’ (139 days) spectrum, we focused on a phase with minimal interference from dust, allowing us to better study the emissions from various elements. The

photoionisation code CLOUDY employs detailed microphysics to simulate the physical conditions of non-equilibrium gas clouds under the influence of an external radiation field. CLOUDY uses 625 species, including ions, molecules, and atoms, and employs five distinct databases for spectral line modelling: STOUT, CHIANTI, LAMDA, H-like and He-like isoelectronic sequences, and the H₂ molecule. All significant ionisation processes, such as photoionisation, Auger processes, collisional ionisation, charge transfer, and various recombination processes (radiative, dielectronic, three-body recombination, and charge transfer), are included self-consistently. For a specified set of input parameters, CLOUDY predicts the intensities and column densities of a large number of spectral lines ($\sim 10^4$) across the electromagnetic spectrum, particularly for non-local thermodynamic equilibrium (NLTE) gas clouds, by solving the equations of thermal and statistical equilibrium in a self-consistent manner. This simulated spectrum can then be compared with the observed spectrum to estimate the physical and chemical characteristics such as the temperature and luminosity of the central ionising source, the density and radii of the ejecta, and the chemical composition of the ejecta. For a detailed description of CLOUDY, see Ferland et al. (2013).

We consider a central ionising source surrounded by a spherically symmetric ejecta whose dimensions are estimated by inner (r_{in}) and outer (r_{out}) radii. The central ionising source is assumed to have a blackbody shape with temperature T (K) and luminosity L (erg s^{-1}). We assume the surrounding ejecta to be clumpy and use the filling factor parameter to set the clumpiness in our CLOUDY models. The filling factor $f(r)$ varies with radius according to the following relation:

$$f(r) = f(r_{in})(r/r_{in})^\beta \quad (5)$$

where r_{in} is the inner radius and β is the power law exponent. The filling factor in novae ejecta typically ranges from 0.01 to 0.1 (Shore 2008). During the early stages, the value is often at the higher end, around 0.1, but decreases over time (Ederolite et al. 2006). In our analysis, we adopted a filling factor of 0.1 for the day 15 spectra, while for the nebular phase spectra, we treated the filling factor as a free parameter. The ejecta density is determined by the total hydrogen number density parameter, $n(r)$ (cm^{-3}), which varies with the radius of the ejecta according to the following relation:

$$n(r) = n(r_{in})(r/r_{in})^\alpha \quad (6)$$

where $n(r)$ is the density at radius r and α is the exponent of power law. In the present study, we have used $\alpha = -3$ for a shell undergoing ballistic expansion and $\beta = 0$, consistent with the values used in previous studies of novae (e.g. Helton et al. 2011; Raj et al. 2018; Pavana et al. 2020; Pandey et al. 2022a,b; Habtie et al. 2024, and references therein). We set the chemical composition of the ejecta by the abundance parameter in CLOUDY. We varied the abundances of only those elements whose emission lines are present in the observed spectra, while we kept the remaining elements at their solar values (Grevesse et al. 2010).

In our CLOUDY models, we used T , L , $n(r)$, and abundances as free input parameters. We employed a wide range of input parameters, varying them in smaller steps throughout the sample space, to generate a comprehensive set of synthetic spectra. We then match these model-generated spectra with the observed spectra to constrain the crucial characteristics of the nova system. After achieving a comparable match with our observations, we referred our attention to the emission lines that originate from

elements such as carbon, oxygen, and nitrogen. Furthermore, we scrutinised the faint lines of sodium, argon, and iron by adjusting the abundances of all elements simultaneously, while allowing for slight variations in temperature, luminosity, and density parameters.

Nova ejecta are known to have an inhomogeneous density distribution, evidenced by the presence of clumps and varying densities within the expanding material (Bode & Evans 2008). In our initial modelling efforts, we found that models with a single uniform density were insufficient to generate emission lines across all transitions. To address this issue, we adopted a two-component density model. The component characterised by high ejecta density produced permitted emission lines in the spectra, while the component with lower ejecta density accounted for the forbidden emission lines. This low density allowed the ionising photons to penetrate deeper into the shell, causing it to become more ionised and hotter (Shore et al. 2003).

It should be noted that our CLOUDY modelling assumes a simple spherically symmetric geometry. In reality, the actual geometry of nova ejecta can be more complex, such as bipolar or irregular shapes. CLOUDY, being a 1D photoionisation code, cannot simulate bipolar and other complex geometries. The assumption of spherical symmetry might oversimplify the actual structure of the ejecta, and this complexity can affect the ionisation and emission properties. We were unable to match the $H\alpha$ line as it was very strong and blended with the [N II] line. Hydrogen Balmer emission lines generally form in the outer region of the ejecta, and our assumption of spherical symmetry might be affecting the modelled strength of the $H\alpha$ emission line (Schwarz et al. 2001). We may be able to test this if the outer regions of the ejecta deviate from this assumption of spherical symmetric geometry. However, the full treatment of non-spherical bipolar geometry is currently out of the scope of this paper. In our future work, we will consider using 3D photoionisation codes which can handle non-spherical geometries. So we will ignore this line, but other lines are generated and match very well.

We also set the covering factor, a measure of how much of the material we can see, for both of these regions in a way that when we add them up, it never exceeds unity. To simplify, we keep most of the details constant for both regions, reducing the number of parameters we need to adjust. The ratios of the lines we model are calculated by adding up the ratios from each region, each multiplied by its covering factor. Finally, we set the inner and outer boundaries of the ejected material based on how fast it is expanding, which we calculate from the width of the emission lines, similar to a previous study by Raj et al. (2018).

As CLOUDY uses many parameters which are interdependent to generate a spectrum, it is difficult to validate the final spectrum visually. Thus, the best-fit model is obtained by calculating χ^2 and reduced χ^2 :

$$\chi^2 = \sum_{i=1}^n \frac{(M_i - O_i)^2}{\sigma_i^2}$$

$$\chi_{red}^2 = \frac{\chi^2}{\nu} \quad (7)$$

M_i and O_i represent the modelled and observed line ratios, respectively. The symbol σ_i denotes the error in the observed flux ratio. The degrees of freedom, denoted by ν , are calculated as $n - n_p$, where n is the number of observed lines, and n_p is the number of free parameters. The observed and modelled flux ratios with the χ^2

Table 2. Observed and best-fit NIR CLOUDY model line flux ratios for day 15 of V5579 Sgr.

| Line ID | λ (um) | Observed ^a | Modelled ^a | χ^2 |
|----------------|----------------|-----------------------|-----------------------|----------|
| <i>J</i> -band | | | | |
| Pa γ | 1.0938 | 7.82E-01 | 5.66E-01 | 7.27E-01 |
| O I + C I | 1.1295 | 1.88E+00 | 1.40E+00 | 2.58E+00 |
| C I | 1.1674 | 3.63E-01 | 1.32E-01 | 5.90E-01 |
| C I | 1.1755 | 6.99E-01 | 1.20E-01 | 3.72E+00 |
| C I | 1.1895 | 3.77E-02 | 6.71E-02 | 9.66E-03 |
| N I | 1.2469 | 1.52E-01 | 1.01E-02 | 2.20E-01 |
| Blnd C I | 1.2575 | 2.54E-01 | 1.60E-01 | 1.42E-01 |
| Pa β | 1.2818 | 1.00E+00 | 1.00E+00 | 0.00E+00 |
| C I | 1.2970 | 1.96E-02 | 5.50E-01 | 3.12E+00 |
| <i>H</i> -band | | | | |
| Br 19 | 1.5256 | 2.22E-01 | 5.57E-01 | 1.24E+00 |
| Br 18 | 1.5341 | 3.00E-01 | 5.95E-01 | 1.39E+00 |
| Br 17 | 1.5439 | 2.80E-01 | 6.39E-01 | 1.42E+00 |
| Br 16 | 1.5557 | 4.85E-01 | 6.88E-01 | 6.63E-01 |
| Br 15 | 1.5685 | 5.51E-01 | 7.46E-01 | 9.46E-01 |
| Br 14 | 1.5881 | 6.95E-01 | 8.14E-01 | 2.27E-01 |
| C I | 1.6005 | 2.66E-01 | 1.92E-01 | 8.54E-02 |
| Br 13 | 1.6109 | 5.91E-01 | 8.96E-01 | 1.04E+00 |
| Br 12 | 1.6407 | 1.00E+00 | 1.00E+00 | 0.00E+00 |
| Br 11 + C I | 1.6865 | 2.33E+00 | 2.83E+00 | 2.69E+00 |
| C I | 1.7045 | 4.48E-01 | 1.43E-01 | 1.03E+00 |
| Br 10 | 1.7362 | 1.38E+00 | 1.31E+00 | 4.56E-02 |
| C I | 1.7448 | 9.48E-01 | 4.37E-01 | 2.91E+00 |
| C I | 1.7672 | 8.72E-01 | 9.18E-01 | 2.36E-02 |
| C I | 1.7790 | 1.48E+00 | 6.14E-01 | 8.38E+00 |
| C I | 1.8022 | 7.92E-01 | 5.11E-01 | 8.83E-01 |
| <i>K</i> -band | | | | |
| C I | 2.1023 | 1.75E-01 | 3.50E-01 | 4.96E-01 |
| Blnd C I | 2.1265 | 4.29E-01 | 8.58E-02 | 1.31E+00 |
| Br γ | 2.1655 | 1.00E+00 | 1.00E+00 | 0.00E+00 |
| Na I | 2.2056 | 6.80E-02 | 2.52E-02 | 2.04E-02 |
| C I | 2.2156 | 2.09E-01 | 3.95E-01 | 3.89E-01 |
| C I | 2.2906 | 1.84E-01 | 4.08E-01 | 5.58E-01 |

values are given in Tables 2 and 3. In general, the error (σ) typically falls within the range of 10% to 30%. This range depends on several factors, including the strength of the spectral line relative to the continuum, the possibility of blending with other spectral lines, uncertainties in de-reddening value, and errors in the measured line flux (Helton et al. 2011; Woodward et al. 2024). We considered σ value of 20% to 30% for the present study.

To make sure our predicted brightness matches the actual observed brightness after accounting for reddening, we assume that V5579 Sgr is about 5.6 kpc away. The measured line brightness is adjusted for reddening, specifically with a value of $E(B - V) = 0.7$ mag, as estimated in Section 3.1. We then compare the adjusted measured brightness with our model's output to calculate χ^2 , which helps us find the best fit.

Table 3. Observed and best-fit optical CLOUDY model line flux ratios for day 1139 of V5579 Sgr.

| Line ID | λ (Å) | Observed ^a | Modelled ^a | χ^2 |
|------------------|---------------|-----------------------|-----------------------|------------|
| [O II] | 3 727 | 4.22E-01 | 3.53E-02 | 1.66E+00 |
| H I | 3 750 | 2.80E-01 | 3.87E-02 | 6.41E-01 |
| H I | 3 798 | 1.10E-01 | 5.88E-02 | 2.97E-02 |
| H I | 3 835 | 8.90E-02 | 7.90E-02 | 1.08E-03 |
| [Ne III] | 3 869 | 3.51E-01 | 8.35E-01 | 2.61E+00 |
| [Ne III] | 3 968 | 3.12E-01 | 2.54E-01 | 5.47E-02 |
| [S II] | 4 069 | 9.86E-02 | 9.68E-02 | 3.70E-05 |
| H I | 4 102 | 4.19E-01 | 2.63E-01 | 2.72E-01 |
| [O III] | 4 363 | 1.28E+00 | 2.73E+00 | 23.51E+00 |
| N III + [Fe III] | 4 640 | 3.76E-01 | 1.36E-01 | 2.66E+00 |
| He II | 4 686 | 3.64E-01 | 4.48E-01 | 1.11E-01 |
| H I | 4 861 | 1.00E+00 | 1.00E+00 | 0.00E+00 |
| [O III] | 4 959 | 9.42E+00 | 9.83E+00 | 2.63E+00 |
| [O III] | 5 007 | 29.56E+00 | 29.31E+00 | 9.60E-01 |
| [Fe VI] | 5 176 | 8.40E-02 | 1.80E-01 | 1.02E-01 |
| [Fe III] | 5 270 | 3.92E-02 | 9.06E-02 | 2.94E-02 |
| He II | 5 412 | 8.12E-02 | 3.65E-02 | 2.22E-02 |
| [Fe VI] | 5 677 | 1.03E-01 | 3.88E-02 | 4.54E-02 |
| [N II] | 5 755 | 8.64E-01 | 7.02E-01 | 4.21E-01 |
| He I | 5 876 | 2.58E-01 | 4.30E-02 | 5.14E-01 |
| [Fe VII] | 6 086 | 1.15E-01 | 3.83E-02 | 6.66E-02 |
| [O I] | 6 300 | 3.78E-01 | 3.54E-01 | 9.86E-03 |
| [O I] | 6 364 | 1.55E-01 | 1.13E-01 | 2.79E-02 |
| H I + [N II] | 6 572 | 8.86E+00 | 3.46E+00 | 323.29E+00 |
| He I | 6 678 | 1.11E-01 | 3.02E-02 | 7.21E-02 |
| He I | 7 065 | 6.10E-02 | 4.470E-02 | 2.18E-03 |
| [Ar III] | 7 136 | 6.90E-02 | 1.90E-01 | 1.65E-01 |
| [Ar IV] | 7 237 | 4.78E-02 | 3.73E-03 | 2.16E-02 |
| He I | 7 281 | 1.60E-02 | 1.01E-02 | 3.80E-04 |
| [O II] | 7 320 | 8.25E-01 | 5.00E-01 | 1.70E+00 |
| [Ar III] | 7 751 | 1.03E-01 | 4.53E-02 | 3.70E-02 |
| He II | 8 237 | 1.55E-02 | 9.90E-03 | 3.53E-04 |
| H I | 8 545 | 2.08E-02 | 6.25E-03 | 2.36E-03 |
| H I | 8 665 | 1.11E-02 | 9.42E-03 | 3.40E-04 |
| H I | 8 750 | 6.62E-03 | 1.18E-02 | 3.04E-04 |
| H I | 8 863 | 8.00E-03 | 1.52E-02 | 5.74E-04 |
| [S III] | 9 069 | 1.46E-01 | 1.88E-01 | 2.84E-02 |
| H I | 9 229 | 8.23E-02 | 2.50E-02 | 3.66E-02 |
| He II | 9 345 | 2.85E-02 | 1.42E-02 | 2.25E-03 |
| [S III] | 9 531 | 2.22E-01 | 4.72E-01 | 1.00E+00 |

^aRelative to H β

To minimise errors related to how we measure brightness at different wavelengths, we use the ratios of modelled and observed prominent hydrogen lines, such as H β in the optical region, P β in *J* band, Br12 in *H* band, and Br γ in *K* band for calibration. This approach helps us to fine-tune our model and improve the accuracy of our predictions.

Table 4. Best-fit NIR CLOUDY model parameters obtained on day 15 for the system V5579 Sgr.

| Parameter | Day 15 |
|--|----------------------------------|
| T_{BB} ($\times 10^4$ K) | 1.58 \pm 0.05 |
| Luminosity ($\times 10^{36}$ erg/s) | 7.76 \pm 0.8 |
| Clump Hydrogen density ($\times 10^{11}$ cm $^{-3}$) | 2.82 |
| Diffuse Hydrogen density ($\times 10^9$ cm $^{-3}$) | 3.55 |
| Covering factor (clump) | 0.60 |
| Covering factor (diffuse) | 0.40 |
| α | -3.00 |
| Inner radius ($\times 10^{14}$ cm) | 1.10 |
| Outer radius ($\times 10^{14}$ cm) | 2.21 |
| Filling factor | 0.1 |
| C/C $_{\odot}$ | 15.5 \pm 3.0 (15) ^a |
| N/N $_{\odot}$ | 40.00 \pm 5 (1) |
| O/O $_{\odot}$ | 32.2 \pm 3.5 (1) |
| Ejected mass ($\times 10^{-4}$ M $_{\odot}$) | 1.67 |
| Number of observed lines (<i>n</i>) | 31 |
| Number of free parameters (<i>n_p</i>) | 9 |
| Degrees of freedom (ν) | 22 |
| Total χ^2 | 36.9 |
| χ^2_{red} | 1.67 |

^aThe number of lines available to obtain an abundance estimate is as shown in the parenthesis.

The abundance values and other parameters obtained from the model are listed in Tables 4 and 5, presented on a logarithmic scale. The results suggest that the levels of helium, oxygen, carbon, and nitrogen are higher compared to solar values. These values are approximations because the calculations rely on only three or four observed lines. The accuracy of abundance solutions is influenced by changes in the opacity and conditions of the ejected material. Despite significant uncertainties, a model with a low chi-square provides a reasonable estimate of abundances. However, the model provides estimates for various parameters, including temperature, luminosity, density, and opacity (as detailed in Tables 4 and 5). These estimates fall within the expected range of values for Fe II novae, even though they should be considered as rough approximations due to the limitations mentioned. The best-fit modelled spectrum (red line) with the corresponding dereddened observed spectrum (black line) is shown in Figs. 8 and 9 in JHK and optical region, respectively. We have calculated the mass of the ejecta within the model shell following Schwarz et al. (2001):

$$M_{shell} = n(r_{in})f(r_{in}) \int_{R_{in}}^{R_{out}} \left(\frac{r}{r_{in}}\right)^{\alpha+\beta} 4\pi r^2 dr \quad (8)$$

The values for density, filling factor, α , and β are adopted from the best-fit model parameters. Estimation of the total ejected shell mass entailed the multiplication of the mass in both density components (clump and diffuse) by their respective covering factors, followed by the addition of these products. The mass of the ejected hydrogen shell is estimated to be 1.67×10^{-4} M $_{\odot}$ and 6.36×10^{-4} M $_{\odot}$ using the modelling results of day 15 and 1 139, respectively. These values are consistent with the theoretical values estimated for CNe (Gehrz et al. 1998).

Table 5. Best-fit optical CLOUDY model parameters obtained on day 1139 for the system V5579 Sgr.

| Parameter | Day 1 139 |
|---|----------------------------------|
| T_{BB} ($\times 10^5$ K) | 2.55 ± 0.10 |
| Luminosity ($\times 10^{36}$ erg/s) | 9.77 ± 0.08 |
| Clump Hydrogen density ($\times 10^6$ cm $^{-3}$) | 5.63 |
| Diffuse Hydrogen density ($\times 10^6$ cm $^{-3}$) | 2.01 |
| Covering factor (clump) | 0.25 |
| Covering factor (diffuse) | 0.75 |
| α | -3.00 |
| Inner radius ($\times 10^{15}$ cm) | 8.91 |
| Outer radius ($\times 10^{16}$ cm) | 1.60 |
| Filling factor | 0.05 |
| He/He $_{\odot}$ | 1.45 ± 0.20 (8) ^a |
| N/N $_{\odot}$ | 22.00 ± 0.30 (2) |
| O/O $_{\odot}$ | 5.8 ± 0.8 (7) |
| Ejected mass ($\times 10^{-4}$ M $_{\odot}$) | 6.36 |
| Number of observed lines (n) | 39 |
| Number of free parameters (n_p) | 10 |
| Degrees of freedom (ν) | 29 |
| Total χ^2 | 39.47 |
| χ^2_{red} | 1.36 |

^aThe number of lines available to obtain abundance estimate is as shown in the parenthesis.

3.5 Dust temperature and mass

A change in slope in the optical light curve about 20 days after the outburst clearly indicates the onset of dust formation (Raj et al. 2011). We anticipate an increase in the fluxes of the NIR band during dust formation. The fact that the H -band flux shows a slight increase, while the K -band flux significantly rises around this time suggests that the dust is self-absorbed (optically thin) in the H -band. We observe a decline, rather than a rise, in the J -band flux during this time, as dust contributes primarily to the K band and beyond. In the present study, we used day 15 and 1 139 spectra for the photoionisation modelling. Based on our best-fit CLOUDY models, the carbon abundance (C/H) was estimated to be 15.5 relative to the solar value on day 15 and decreased to its solar value on day 1 139. In contrast, the oxygen abundance (O/H) was estimated to be 32.2 on day 15 and decreased to 5.8 relative to the solar value during the subsequent phase, indicating that the ejecta could be rich in oxygen. The decrease in carbon abundance can be attributed to its depletion in dust grain formation. Theoretical hydrodynamic models of the TNR also suggest that the gas phase of the nova ejecta has a relatively higher abundance of oxygen (O). This is because an environment where oxygen (O) is higher than carbon (C) may also make it easier for carbon-rich dust grains to form (Starrfield, Iliadis, & Hix 2016).

To estimate the outburst luminosity, we have used the $(\lambda F_{\lambda})_{max}$ values for optical and IR from Raj et al. (2011). Using the relation given by Gehrz (2008) that the outburst luminosity is equal to $4.11 \times 10^{17} d^2 (\lambda F_{\lambda})_{max} L_{\odot}$. We calculate the outburst luminosity (L_O) on day 5 and IR dust luminosity on day 26 (L_{IR}) to be $4.59 \times 10^5 L_{\odot}$ and $3.12 \times 10^4 L_{\odot}$, respectively, using distance $d = 5.6$ kpc. The inferred visible optical depth ($\tau = \frac{L_{IR}}{L_O}$) is calculated to be 0.07, indicating the presence of thin optical dust emission

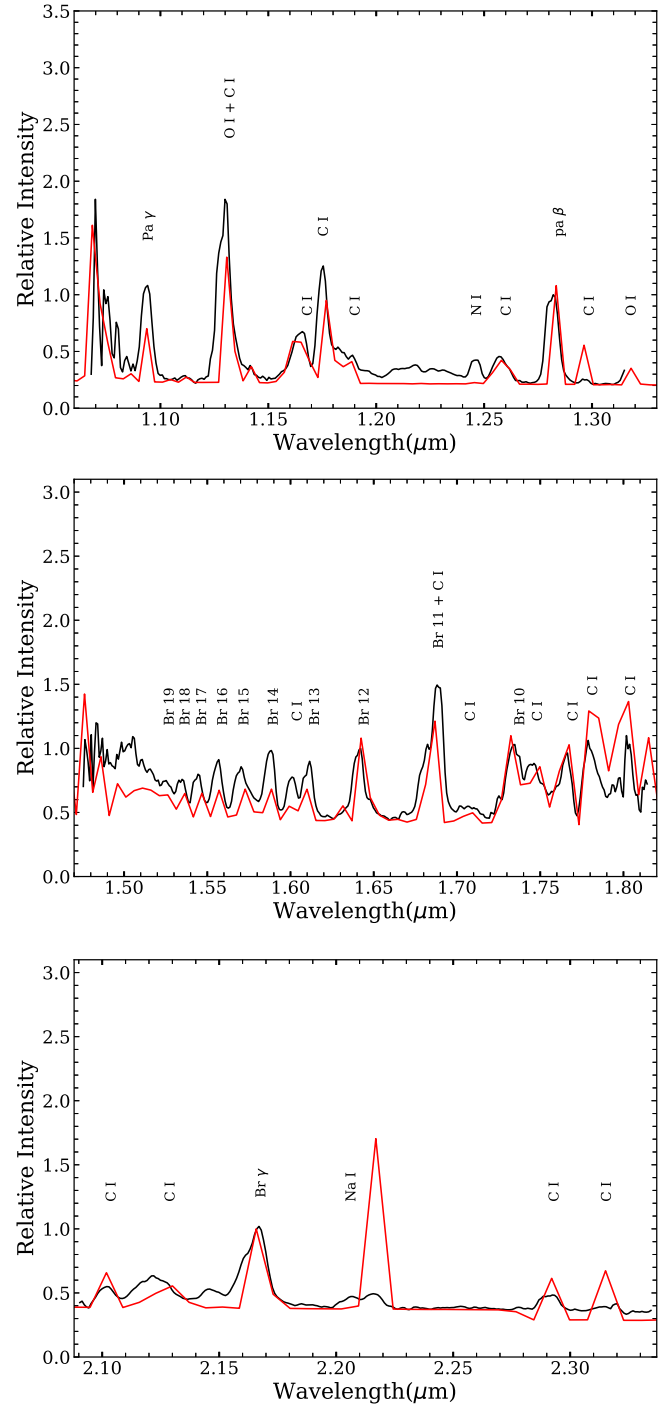


Figure 8. Best-fit CLOUDY synthetic spectrum (red line) plotted over the observed spectrum (black line) for JHK bands obtained on 2008 May 3 (day 15).

during the early dust formation phase. Similar values were previously determined for V1668 Cyg (Gehrz 1988) and V1831 Aql (Banerjee et al. 2018). Banerjee et al. (2018) suggested that small τ values imply either clumpy dust distribution, hence does not cover all angles of the sky towards the nova as seen by the observer or a homogeneous dust shell with insufficient material to achieve optical thickness.

Dust condensed in the ejecta of V5579 Sgr as early as $\simeq +20$ d after outburst (Russell et al. 2008). The TReCs spectrum on

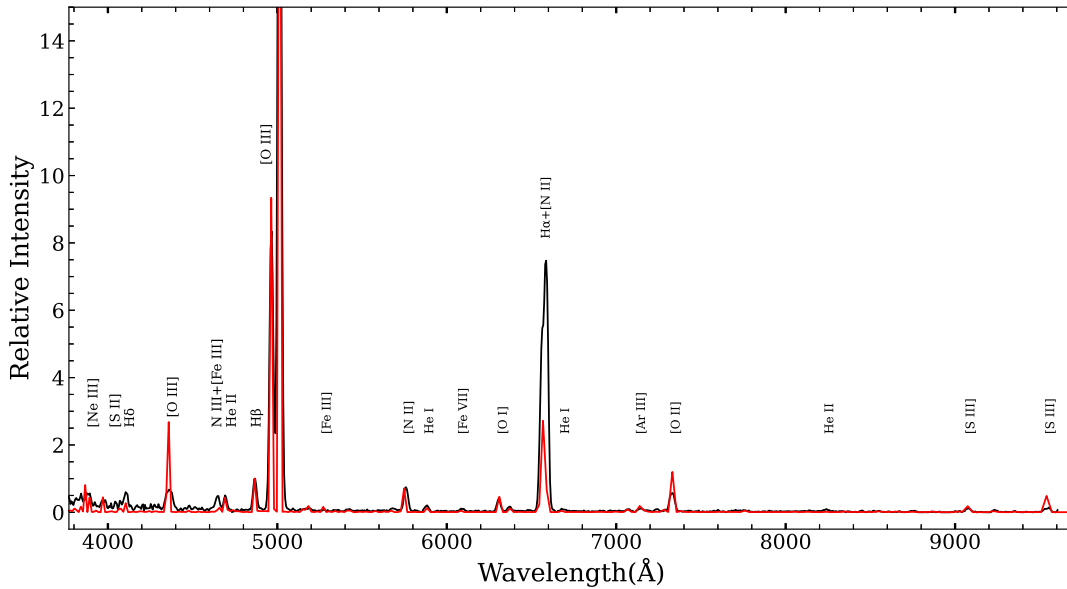


Figure 9. Best-fit CLOUDY synthetic spectrum (red line) plotted over the observed spectrum (black line) of V5579 Sgr obtained on 2011 June 2 (day 1 139).

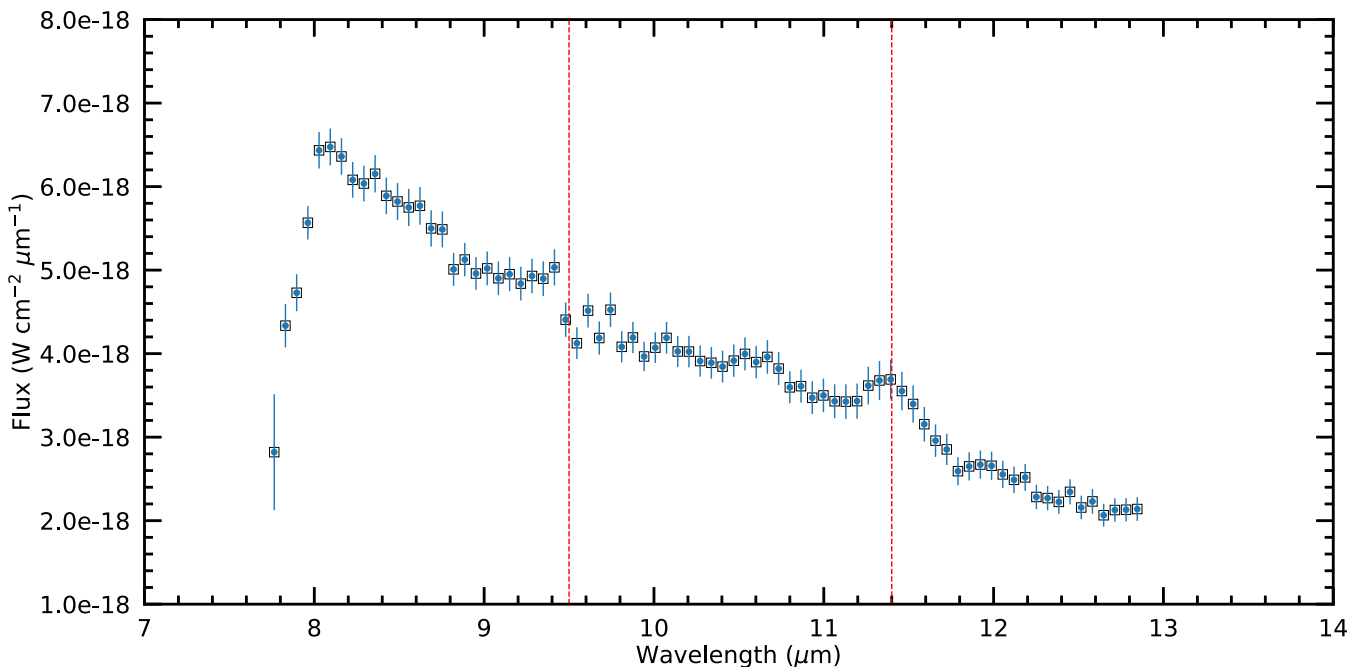


Figure 10. The 7.70–14.00 μm low-resolution ($R \simeq 120$) spectrum of V5579 Sgr obtained on Gemini-S (+TReCS) on 2009 Sept 23. (Day +522.26). The vertical dashed red lines are the (PAHs; Allamandola, Tielens & Barker 1989) complexes detected in the NASA Spitzer spectra of V2362 Cygni. The slope of the observed TReCS spectrum of V5579 Sgr follow that of the Rayleigh-Jeans tail of a hot blackbody arising from condensed dust in the ejecta (e.g. Rudy et al. 2008; Raj et al. 2011).

$\simeq 522$ d (Fig. 10) show that emission from dust is still present at this late epoch. The Rayleigh Jean tail of the hot blackbody emission arising from carbonaceous grains (which have featureless spectral energy distributions (SEDs) in the IR Draine & Li 2007) has spectral features superposed on the otherwise smooth continuum. In V5579 Sgr, there are spectral features evident in the SED at 9.5 and 11.4 μm (see Fig. 10) associated with Polycyclic Aromatic

Hydrocarbon (PAH) like features seen in the V2362 Cygni (Helton et al. 2011) and in V705 Cas (Eyres et al. 1997). V5579 Sgr thus joins the growing list of novae where such materials have formed.

The observations from the Wide field Infrared Survey Explorer (WISE; Wright et al. (2010)) also support emission from the dust at longer wavelengths (see Fig. 11). We estimate the temperature of the dust shell around 702 days after the outburst by using the

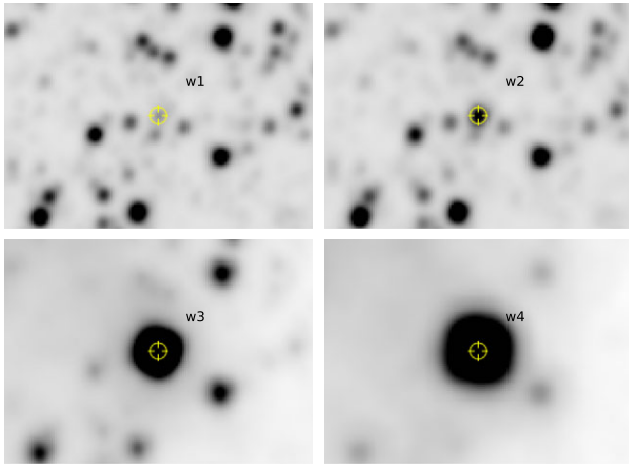


Figure 11. A mosaic of a 3×3 arc minute square field around V5579 Sgr. The source is detected in all 4 WISE bands: W1 ($3.4 \mu\text{m}$), W2 ($4.6 \mu\text{m}$), W3 ($12 \mu\text{m}$), and W4 ($22 \mu\text{m}$); the emission at the longer W3 and W4 bands is very pronounced. The WISE images were taken in March 2010 (more details in Section 3.5), nearly 2 yr since discovery. Although the nova had faded below 15 mag in the V band by this time (see Fig. 1), it remained strikingly bright in the near and mid-IR due to emission from newly formed dust in the ejecta.

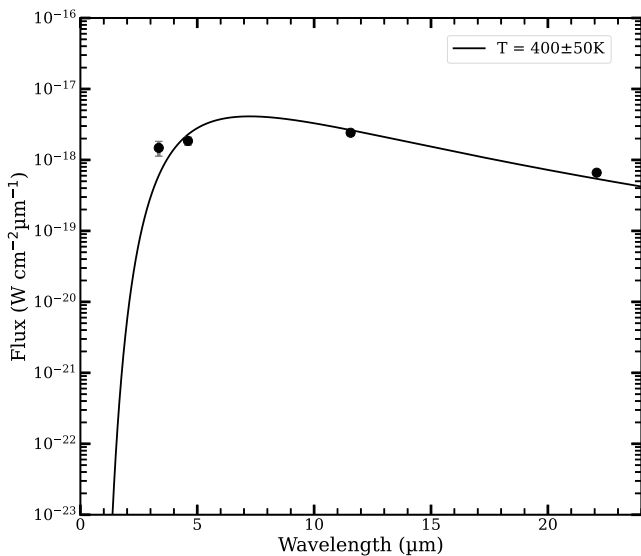


Figure 12. The SED shows a blackbody fit to the WISE data taken on 2010 March 22 with a temperature of about 400 K.

WISE magnitudes as 400 ± 50 K. However, the temperature estimate for the dust shell may have a large uncertainty, as we assume that the isothermal dust and we have used only four wavelengths to fit the SED where the dust could contribute at larger wavelengths beyond $22 \mu\text{m}$.

The mass of the dust shell is calculated from the SED on 22 March 2010 shown in Fig. 12. We estimate the dust mass following Evans et al. (2017) and Banerjee et al. (2018), assuming that the grains are spherical and that the dust is composed of carbonaceous material. Using the relations given by Evans et al. (2017), we find that the dust masses for amorphous carbon (AC) and graphitic carbon (GR) grains are as follows. For optically thin AC,

$$\frac{M_{\text{dust-AC}}}{M_{\odot}} \simeq 5.83 \times 10^{17} \frac{(\lambda f_{\lambda})_{\text{max}}}{T_{\text{dust}}^{4.754}} \quad (9)$$

and for optically thin graphitic carbon,

$$\frac{M_{\text{dust-GR}}}{M_{\odot}} \simeq 5.19 \times 10^{19} \frac{(\lambda f_{\lambda})_{\text{max}}}{T_{\text{dust}}^{5.315}} \quad (10)$$

where we assume the distance $D = 5.6$ kpc, the density of the carbon grains $\rho = 2.25 \text{ gm cm}^{-3}$, and $(\lambda f_{\lambda})_{\text{max}}$ is in unit of W m^{-2} . The dust mass, which is independent of grain size (Evans et al. 2017), is estimated to be $\sim 8.3 \times 10^{-8} M_{\odot}$ and $2.6 \times 10^{-7} M_{\odot}$, for AC and GR grains, respectively. AC grains provide a much better fit across a wider temperature range (400–1700 K) compared to graphitic carbon, which shows a reasonably good fit only within the narrower range of 700–1500 K (Blanco, Falcicchia, & Merico 1983). This finding suggests that the dust grains in the nova are probably composed mainly of AC. The value of masses show that a large amount of optically thick dust was formed after May 2008 in the nova ejecta.

The dust mass might not be totally accurate for some reasons as the dust might have only formed in some parts of the ejecta, not everywhere, and the temperatures we measured might not be totally accurate. The dust's ability to emit light depends on composition and the size of the dust grain, and this can make a difference in how we see its temperature (Kruegel 2003).

4. Discussion

The observed NIR excess suggests that a large amount of optically thick dust was formed in the nova ejecta. After a peak was reached, the J-H and H-K colours started to show a downward trend, indicating either the destruction of the dust molecules due to radiation from the central source or the thinning of the dust shell as it expands and becomes less evident. A similar behaviour was seen in V2676 Oph where molecule formation before dust condensation was reported and had similar colours, J-K = 8, J-H = 4.5, and H-K = 3.8 mag (Raj et al. 2017). Dust formation in CNe is an intriguing phenomenon in astrophysics because the nova forms dust within several days to several tens of days after the explosion (TNR) and ejects the molecules and dust grains, including PAH, into galactic space (Gehrz et al. 1998). Understanding the location of the dust condensation layer is very important to understand dust formation in CNe.

Usually, the chemical composition of the stellar atmosphere determines the type of dust that forms in the stellar ejecta. Studies have shown that a higher ratio of carbon to oxygen ($C > O$) is necessary for the formation of silicon carbide (SiC) and AC grains. This is because CO is the most stable molecule at $T < 2000$ K, at which grains usually form. As the CO molecule once formed in the ejecta, all of the remaining oxygen was trapped in the CO molecule, leaving only residual carbon available for grain formation. In contrast, when oxygen predominates over carbon ($O > C$), the carbon is locked up in CO formation, while remaining oxygen tends to combine with other elements to form oxides and silicates (Waters 2004). However, it has been observed that some novae are capable of producing significant amounts of both carbon-rich and oxygen-rich dust grains. Examples of such cases are V705 Cas (Evans et al. 2005), V1065 Cen (Helton et al. 2011), V5668 Sgr (Gehrz et al. 2018), V1280 Sco (Pandey et al. 2022a), etc. This may imply that the CO formation process does not reach saturation in the nova ejecta, thereby permitting the incorporation of both carbon and oxygen into the dust. On the other hand, this could also

mean that there are differences in the amounts of carbon and oxygen in the ejecta, which would cause the carbon-to-oxygen (C:O) ratio to vary depending on where it is found. The exact mechanism for the presence of this bimodal dust in nova ejecta is not well known (Starrfield et al. 2016; Sakon et al. 2016).

V5579 Sgr belongs to the fast novae speed class ($t_2 \sim 9$ days) with small fluctuations in the NIR light curve in the early phase followed by a decline in the late phase. In the optical light curve, from day 20 a decline is seen due to dust formation. Only nova Cyg 2006 (V2362 Cyg) and nova Aql 1995 (V1425 Aql) formed an optically thin dust with a similar value for t_2 . But V2362 Cyg showed a pre-maximum rise lasting for about 2.8 days and also a second maximum at $\Delta t = 239$ d, after the optical maximum and dust formed around $\Delta t = 251$ d. In the case of V1425 Aql there was an indication of dust in the ejecta around $\Delta t = 22$ d, while the present observations show that dust formation occurred even earlier around $\Delta t = 15$ d after the optical maximum in V5579 Sgr. Thus the IR data presented here for V5579 Sgr along with the results of Kamath et al. (1997) on V1425 Aql indicate that the earliest dust formation time scale for an Fe II nova lies in the range of 15–22 days.

Our CLOUDY modelling supports the notion of a nitrogen enrichment in the V5579 Sgr nova ejecta, likely due to proton capture during thermonuclear runaway (TNR). This finding aligns with observations of other novae, such as V705 Cas, where Hauschildt et al. (1994) reported an enhancement of heavy elements (particularly carbon, nitrogen, and oxygen) compared to solar abundances. Shore et al. (2018) explored the potential consequences of a significantly elevated nitrogen-to-carbon (N/C) ratio, particularly its influence on dust formation in CO-type novae. The overall increase in heavy element abundance within the ejecta can potentially disrupt the thermal balance of the gas, fostering conditions that favour the formation of dust nucleation sites. As suggested Ferland & Shields (1978), a higher metallicity allows for more efficient cooling of the ejecta, facilitating the achievement of thermal equilibrium at lower kinetic temperatures.

5. Summary

We have presented a comprehensive optical spectrophotometric and NIR photometric evolution. The important results of the analyses are summarised here.

1. Using optical and NIR data from AAVSO and SMARTS, t_2 was estimated to be 9 ± 0.2 d, indicating that V5579 Sgr belongs to the class of fast novae.

2. The reddening $E(B - V)$ was estimated to be about 0.7 ± 0.14 and the distance to the nova was found to be 5.6 ± 0.2 kpc. Using MMRD relation we have estimated the absolute magnitude of the nova M_v to be 9.3 ± 0.1 .

3. The mass of WD was estimated to be $1.16 M_\odot$.

4. The spectral evolution clearly indicates that it belongs to the Fe II class of novae. The nova evolves in PFeAo sequence as per the classification given by Williams et al. (1991). Coronal lines are absent in the optical spectrum during the late phase.

5. We utilised the CLOUDY photoionisation code to simulate the optical and near-IR spectra of the dust-forming nova V5579 Sgr. From the best-fit model, we estimate various physical and chemical parameters of the system. Our abundance analysis shows that the ejecta are significantly enhanced relative to solar, $O/H = 32.2$, $C/H = 15.5$, and $N/H = 40.0$ in the early decline phase and $O/H = 5.8$, $He/H = 1.5$, and $N/H = 22.0$ in the nebular phase.

6. The low-resolution mid-IR Gemini spectra obtained 522 days since discovery showed PAH-like features. Using the WISE magnitudes, we found that the temperature of the dust is approximately 400 ± 50 K on day 702. The dust mass is estimated to be $\sim 8.3 \times 10^{-8} M_\odot$ and $2.6 \times 10^{-7} M_\odot$, for AC and GR grains, respectively.

Acknowledgement. The authors would like to thank the referee for critically reading the manuscript and providing valuable suggestions to improve it. We acknowledge with thanks the variable star observations from the AAVSO International Database contributed by observers worldwide and used in this research. We also acknowledge the use of SMARTS data. R Pandey acknowledges the Physical Research Laboratory, Ahmedabad, India, for her post-doctoral fellowship.

Based on observations obtained at the international Gemini Observatory, a program of NSF NOIRLab, acquired through the the Gemini Science Archive prior to December 2015 [GS-2009B-Q68], which is managed by the Association of Universities for Research in Astronomy (AURA) under a cooperative agreement with the U.S. National Science Foundation on behalf of the Gemini Observatory partnership: the U.S. National Science Foundation (United States), National Research Council (Canada), Agencia Nacional de Investigación y Desarrollo (Chile), Ministerio de Ciencia, Tecnología e Innovación (Argentina), Ministério da Ciência, Tecnologia, Inovações e Comunicações (Brazil), and Korea Astronomy and Space Science Institute (Republic of Korea).

Data Availability. No data or material or software are required for sharing.

References

- Allamandola, L. J., Tielens, A. G. G. M., & Barker, J. R. 1989, *ApJS*, 71, 733 (ISSN 0067-0049). Research supported by NASA, DOE, and NSF.
- Banerjee, D. P. K., Srivastava, M. K., Ashok, N. M., Munari, U., Hamsch, F.-J., Righetti, G. L., & Maitan, A. 2018, *MNRAS*, 473, 1895.
- Blanco, A., Falcicchia, G., & Merico, F. 1983, *Ap&SS*, 89, 163.
- Bode, M. F., & Evans, A. 2008, *Classical Novae*, Vol. 43. <https://doi.org/10.1017/CBO9780511536168>.
- Chatzikos, M., et al. 2023, *RMxAA*, 59, 327. <https://doi.org/10.22201/ia.01851101p.2023.59.02.12>.
- De Buizer, J. M., & Scott Fisher, R. 2005, in *High Resolution Infrared Spectroscopy in Astronomy* (Berlin, Heidelberg: Springer Berlin Heidelberg), 84. ISBN: 978-3-540-31606-0.
- Downes, R. A., & Duerbeck, H. W. 2000, *AJ*, 120, 2007.
- Draine, B. T., & Li, A. 2007, *ApJ*, 657, 810.
- Dvorak, S., Guido, E., & Sostero, G. 2008, *Central Bureau Electronic Telegrams*, Vol. 1342, 2.
- Ederoclite, A., et al. 2006, *A&A*, 459, 875.
- Evans, A., et al. 2017, *MNRAS*, 466, 4221.
- Evans, A., Tyne, V. H., Smith, O., Geballe, T. R., Rawlings, J. M. C., & Eyres, S. P. S. 2005, *MNRAS*, 360, 1483.
- Eyres, S. P. S., Evans, A., Geballe, T. R., Davies, J. K., & Rawlings, J. M. C. 1997, *ASS*, 251, 303. <https://doi.org/10.1023/A:1000787528827>.
- Ferland, G. J., et al. 2013, *RMxAA*, 49, 137.
- Ferland, G. J., & Shields, G. A. 1978, *ApJ*, 226, 172.
- Gehrz, R. D., et al. 2018, *ApJ*, 858, 78.
- Gehrz, R. D., Truran, J. W., Williams, R. E., & Starrfield, S. 1998, *PASP*, 110, 3.
- Gehrz, R. D. 1988, *ARA&A*, 26, 377. <https://doi.org/10.1146/annurev.aa.26.090188.002113>.
- Gehrz, R. D. 2008, in *Classical Novae*, Cambridge Astrophysics, ed. M. F. Bode, & A. Evans, 167 (Cambridge University Press).
- Grevesse, N., Asplund, M., Sauval, A. J., & Scott, P. 2010, *ASS*, 328, 179. <https://doi.org/10.1007/s10509-010-0288-z>.
- Habtie, G. R., Das, R., Pandey, R., Ashok, N. M., & Dubovsky, P. A. 2024, *MNRAS*, 527, 1405.
- Hachisu, I., & Kato, M. 2007, *ApJ*, 662, 552.
- Hachisu, I., & Kato, M. 2019, *ApJS*, 242, 18.

- Hachisu, I., & Kato, M. 2021, *ApJS*, 253, 27.
- Harker, D. E., Woodward, C. E., Kelley, M. S. P., & Wooden, D. H. 2018, *AJ*, 155, 199.
- Hauschildt, P. H., Starrfield, S., Shore, S. N., Gonzalez-Riestra, R., Sonneborn, G., & Allard, F. 1994, *AJ*, 108, 1008.
- Helton, L. A., et al. 2010, *AJ*, 140, 1347.
- Helton, L. A., Evans, A., Woodward, C. E., & Gehrz, R. D. 2011, in *EAS Publications Series*, Vol. 46, ed. C. Joblin, & A. G. G. M. Tielens (EAS Publications Series), 407. <https://doi.org/10.1051/eas/1146042>.
- Henden, A., & Munari, U. 2008, *IBVS*, 5834, 1.
- Iijima, T., & Naito, H. 2011, *A&A*, 526, A73.
- José, J., Shore, S. N., & Casanova, J. 2020, *A&A*, 634, A5. <https://doi.org/10.1051/0004-6361/201936893>.
- Jurdana-Sepic, R., & Munari, U. 2008, *IBVS*, 5839, 1.
- Kafka, S., 2021. Observations from the AAVSO International Database.
- Kamath, U., Anupama, G. C., Ashok, N., & Chandrasekhar, T. 1997, *AJ*, 114, 2671. <https://doi.org/10.1086/118677>.
- Kiss, L. L., & Thomson, J. R. 2000, *A&A*, 355, L9.
- Kruegel, E. 2003, *The Physics of Interstellar Dust*.
- Livio, M. 1992, *ApJ*, 393, 522 (ISSN 0004-637X). Research supported by Space Telescope Science Institute.
- Munari, U., Siviero, A., Moretti, S., Tomaselli, S., Maitan, A., Castellani, F., Dallaporta, S., & Ochner, P. 2008, *Central Bureau Electronic Telegrams*, 1352, 1.
- Munari, U., et al. 2008, *A&A*, 492, 145.
- Nakano, S., et al. 2008, *International Astronomical Union Circular*, 8937, 1.
- Osterbrock, D. E., & Ferland, G. J. 2006, *Astrophysics of Gaseous Nebulae and Active Galactic Nuclei* (Sausalito, CA: University Science Books).
- Pandey, R., Das, R., Shaw, G., & Mondal, S. 2022a, *ApJ*, 925, 187.
- Pandey, R., Habtie, G. R., Bandyopadhyay, R., Das, R., Teyssier, F., & Fló, J. G. 2022, *MNRAS*, 515, 4655.
- Pavana, M., Raj, A., Bohlsen, T., Anupama, G. C., Gupta, R., & Selvakumar, G. 2020, *MNRAS*, 495, 2075.
- Raj, A., Ashok, N. M., & Banerjee, D. P. K. 2011, *MNRAS*, 415, 3455.
- Raj, A., Das, R. K., & Walter, F. M. 2017, *ApJ*, 835, 274.
- Raj, A., Pavana, M., Kamath, U. S., Anupama, G. C., & Walter, F. M. 2018, *AcA*, 68, 79. ISSN: 00015237. <https://doi.org/10.32023/0001-5237/68.1.4>.
- Rudy, R. J., Lynch, D. K., Russell, R. W., Crawford, K., Kaneshiro, B., Woodward, C. E., Sitko, M., & Skinner, M. 2008, *International Astronomical Union Circular*, 8952, 2.
- Russell, R. W., Rudy, R. J., Lynch, D. K., Woodward, C. E., Marion, H., & Griep, D. 2008, *V5579 Sagittarii*, 8948, 1.
- Sakon, I., et al. 2016, *ApJ*, 817, 145.
- Schwarz, G. J., et al. 2011, *ApJS*, 197, 31.
- Schwarz, G. J., Shore, S. N., Starrfield, S., Hauschildt, P. H., Della Valle, M., & Baron, E. 2001, *MNRAS*, 320, 103.
- Shore, S. N., Paul Kuin, N., Mason, E., & De Gennaro Aquino, I. 2018, *A&A*, 619, A104.
- Shore, S. N., et al. 2003. *AJ*, 125, 1507.
- Shore, S. N. 2008, in *Classical Novae*, ed. M. F. Bode, & A. Evans, *CAMBRIDGE Astrophysics* (Cambridge University Press), 194.
- Starrfield, S., Bose, M., Iliadis, C., Raphael Hix, W., Woodward, C. E., & MarkWagner, R. 2020, *ApJ*, 895, 70. <https://doi.org/10.3847/1538-4357/ab8d23>.
- Starrfield, S., Iliadis, C., & WRHix 2016, *PASP*, 128, 051001.
- Strope, R. J., Schaefer, B. E., & Henden, A. A. 2010, *AJ*, 140, 34.
- Wallace, P. T. 1994, *Astronomical Data Analysis Software and Systems III*, 61, 481.
- Walter, F. M., Battisti, A., Towers, S. E., Bond, H. E., & Stringfellow, G. S. 2012, *PASP*, 124, 1057.
- Warner, B. 1995, *Cataclysmic Variable Stars*, Vol. 28.
- Warner, B. 2008, *Cambridge Astrophysics Series*, Vol. 43, 16.
- Waters, L. B. F. M. 2004, in *Astrophysics of Dust*, ed. A. N. Witt, G. C. Clayton, & B. T. Draine, *ASTRONOMICAL Society of the Pacific Conference Series*, 309, 229.
- Williams, R. E. 1994, *ApJ*, 426, 279 (ISSN 0004-637X).
- Williams, R. E., Hamuy, M., Phillips, M. M., Heathcote, S. R., LisaWells, & Navarrete, M. 1991, *ApJ*, 376, 721 (ISSN 0004-637X).
- Woodward, C. E., Shaw, G., Starrfield, S., Evans, A., & Page, K. L. 2024, *ApJ*, 968, 31. <https://doi.org/10.3847/1538-4357/ad4097>.
- Wright, E. L., et al. 2010, *AJ*, 140, 1868.
- Yamaoka, H., Haseda, K., & Fujii, M. 2008, *Central Bureau Electronic Telegrams*, Vol. 1344, 1.